SUPPLEMENTAL MATERIAL

Single-Slit Electron Diffraction with Aharonov-Bohm Phase: Feynman's Thought Experiment with Quantum Point Contacts

Pradip Khatua,[1,2] Bhavtosh Bansal,[2] and Dan Shahar[1]

[1]*Department of Condensed Matter Physics, Weizmann Institute of Science, Rehovot 76100, Israel*

[2]*Indian Institute of Science Education & Research Kolkata, Mohanpur Campus, Nadia 741252, West Bengal, India*

I. SAMPLE DETAILS AND ITS CHARACTERIZATIONS

The low temperature electrical characterization was carried out in photolithographically defined Hall bars patterned from a conventional modulation doped GaAs/AlGaAs heterojunction forming a two-dimensional electron gas (2DEG). The 2DEG was located 100 nm below the insulating cap layer. Ohmic contacts were made by depositing Ni(5 nm)/Ge(75 nm)/Au(150 nm)/Ni(45 nm) and alloying them at 460^o C for 1 minute. Hall effect and magneto-resistance were measured in dilution refrigerator at $\sim$ 10 mK temperature. The four-terminal resistances R_{xx} and R_{xy} were measured by standard lock-in technique using AC current of amplitude 1 nA and frequency 11.4 Hz. From the Hall measurement, the sheet electron density (n_s) of the material was measured to be $\sim 1.21 \times 10^{11}$ cm^{-2}. The mobility (μ) at such low temperature was $\sim 1.72 \times 10^6$ cm^2/V-s, which corresponds to an electron mean-free-path $l_{\rm mfp} \sim 10\,\mu$m and Fermi wavelength $\lambda_F \approx 73$ nm.

A scanning electron micrograph of the device is shown in Fig. 1 (supplementary). The device was fabricated by standard electron-beam and photo-lithography techniques. For

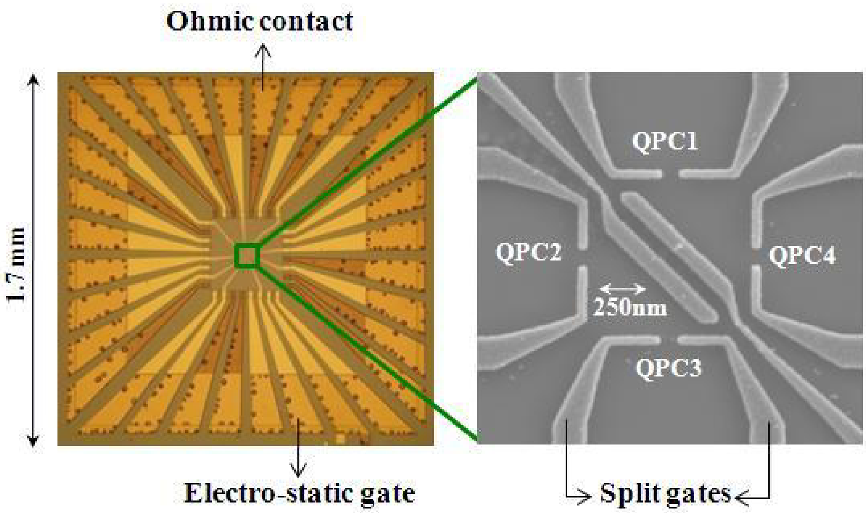

FIG. 1: (supplementary) Optical microscope image of the real device along with its Ohmic contacts and electrostatic gates. Scanning electron micrograph (SEM) of the device is shown on the right side. The metallic split gates together form a QPC on application of electrostatic voltage at the Schottky gates. The two long diagonal gates traversing the detector space were not used in the measurements.

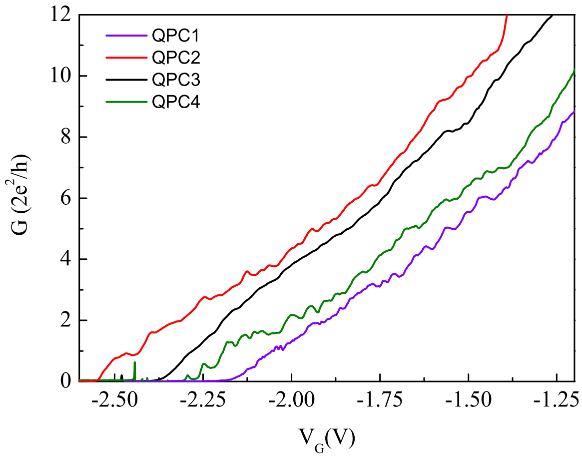

FIG. 2: (supplementary) Plots of the conductance G *vs.* gate voltage V_G for the four QPCs at 10 mK. QPC is formed when $V_G < -1$ V.

injecting or detecting the electrons, several split-gate quantum point contacts (QPC) along with Ohmic contacts were made with four QPC's on the four arms of a $1\mu m$ square. The metal gate structures [Ti(5 nm)/Au(100 nm)] were deposited on the insulating cap layer. The width (W) and channel length (L_x) of the QPC's were 150 nm and 65 nm respectively. The QPC's were formed by applying electrostatic potential on these split-gate metal structures (Schottky gates). The device was ultrasonically bonded by using Au wires and the measurement was carried out at 10 mK temperature.

The characteristics of each QPC[1] were tested individually by four terminal conductance measurements with 1 nA current across the constrictions as a function of the split-gate voltages. Fig. 2 (supplementary) shows the plots of conductance G *vs.* applied gate voltage V_g for three QPC's (QPC1, QPC2, and QPC4). Below -1.2 V, the conductance varies almost continuously as the QPC's are gradually pinched off. The QPC channel length L_x in our device is comparable to the Fermi wavelength λ_F. Steps in conductance are normally observed when $L_x \gg \lambda_F$.[2,3] Nonetheless, given the high mobility and ultralow temperature, the transport at the QPC is safely believed to be ballistic. Complete transmission of each mode should correspond to a conductance of $\sim \frac{2e^2}{h}$ for the slit width of $\sim \frac{\lambda_F}{2}$ and the number of modes can be controlled simply by changing V_G.[1,4] The alignment of two opposite QPCs was tested by measuring beam collimation in a varying magnetic field using one of them as

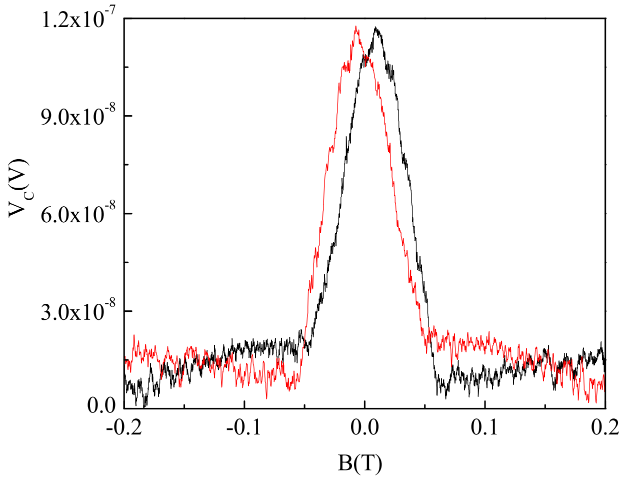

FIG. 3: (supplementary) Collector voltage (V_C) vs. magnetic field (B) corresponding to the cases when one of the QPC's between QPC2 and QPC4 was used as an injector and the other as detector and vice versa. The QPC alignment is tested for gate voltages of $-1.25V$ at the injector QPC, corresponding to 10 modes.

injector and the other as detector and then reversing their roles. A typical result of such test is shown in Fig. 3 (supplementary). The choice of QPC split gate voltages were such that the channel width allowed for about 10 conducting modes through both the injector and two modes in the detector QPC. Typically, the noise level in the measurement of the collector voltage V_C was about 10 nV, as is evident from the background signal beyond 0.05 T magnetic field in Fig. 3 (supplementary).

In Fig. 4 (supplementary), we show the signal measured by the detector QPC4 for current injected by QPC2 as a function of magnetic field. QPC2 is set for different gate voltages, as mentioned in the figure, meaning different modes are allowed to transmit through it. A diffraction pattern was obtained only when up to two modes were present at the injector QPC. As the number of modes at the injector QPC were increased, only coherent electron beam collimation was detected.[5] The distance between the injector and detector QPCs was found to be very critical for clearly observing modulation in the measured nonlocal voltage. Nevertheless, we could detect the diffraction pattern with contributions from up to five modes by reducing the injector to detector distance to $L/\sqrt{2} \sim 0.7\,\mu$m in the 45^o configuration.

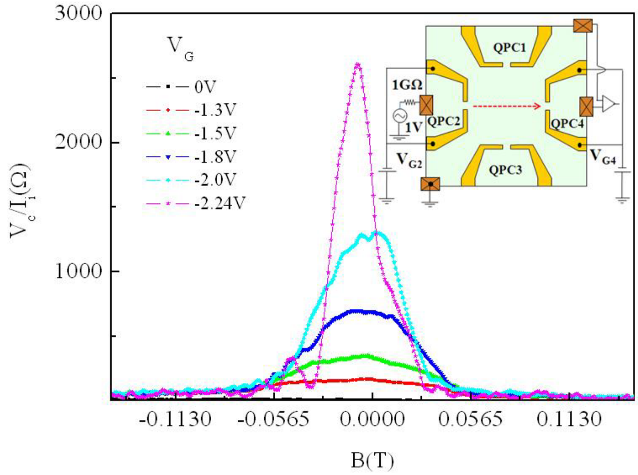

FIG. 4: (supplementary) Signal measured at the detector QPC4 while current is injected through QPC2 in presence of magnetic field perpendicular to the plane of the sample. Circuit diagram for the measurement is shown in the inset.

II. ELECTRON DIFFRACTION FROM SMALL APERTURES IN PRESENCE OF WEAK MAGNETIC FIELD

Eq. 2 (main text) were supported with very qualitative arguments. It can be derived more rigorously. The experimental configuration of our work has already been dealt with theoretically by Saito, et al. using a fully quantum mechanical Green function analysis.[6] So rather than reproducing the somewhat involved calculation, we will just sketch the main arguments of the derivation leaving out the details, with the aim of comparing this more rigorously derived formula with Eq. 2 (main text). We find that our very sketchy extension of Feynman's argument for electron double-slit interference experiment is indeed correct.

The diffraction problem for the electron wave can be formulated as a Dirichlet boundary value problem for the Schrodinger equation. In our experiments, there are two complications as compared to the standard description of scalar wave diffraction theory in the far field.[7] Firstly, the electrons are subjected to a (non-quantizing) magnetic field whose effect on the electron phase must be rigorously taken into account. Secondly, the size of the aperture is comparable to the wavelength of the electrons. The second point is more subtle which we comment upon in the next subsection below.

For a 2DEG at low temperature, one need only consider a two-dimensional geometry

$[f(\mathbf{r}) = f(x,y)]$ in the xy-plane, where the right half-plane (our region of interest) is separated from the left half-plane by a boundary formed by an infinite wall (line) at $x = 0$ [Fig. 5 (supplementary)]. This wall has a small orifice (QPC) around $y = 0$, whose effective size is varied by the gate voltage V_g. By construction, the Dirichlet Green function $G^+(\mathbf{r}', \mathbf{r}) = 0$ if $\mathbf{r}$ or $\mathbf{r}'$ is a point on the boundary. If the value of the wave function $\psi(\mathbf{r}) = \phi(0, y)$ is known on the $x = 0$ boundary and falls off at infinity, then the value of the wave function anywhere on the right half-plane $(y, x > 0)$ is unambiguously determined by the following equation:

$$\psi(\mathbf{r}') = \frac{i}{2m^*} \int_{boundary} dS\ \hat{n}(\mathbf{r})[\phi(\mathbf{r})(-i\hbar\nabla_r G^+(\mathbf{r}', \mathbf{r}))]. \tag{1}$$

$\hat{n}(\mathbf{r})$, the unit vector normal to the boundary, is in the present case along the x-direction. The measured diffraction pattern is just $|\psi(\mathbf{r}')|^2$ where $\mathbf{r}' = (x', y')$ is the position of the detector.

A. Writing B≠0 Green function $G^+(\mathbf{r}', \mathbf{r})$ in terms of 2D Green functions $G^0(\mathbf{r}', \mathbf{r})$ for free propagation

The derivation of $G^+(\mathbf{r}', \mathbf{r})$ involves two steps. First, one can write $G^+(\mathbf{r}', \mathbf{r})$ in terms of the Dirichlet Green function $G^0(\mathbf{r}', \mathbf{r})$ for $B = 0$ diffraction problem in the same geometry.

$$G^+(\mathbf{r}', \mathbf{r}) = e^{i\theta(\mathbf{r}', \mathbf{r})} G^0(\mathbf{r}', \mathbf{r}). \tag{2}$$

$\theta(\mathbf{r}', \mathbf{r})$ is the Aharanov-Bohm phase[8] accumulated by the Green function along the path from $\mathbf{r}$ to $\mathbf{r}'$ defined by the curve C. The curve $C(\mathbf{r} \to \mathbf{r}')$ is determined connecting together the tangents to the gradient vector of the $B = 0$ Green function at points between $\mathbf{r}$ and $\mathbf{r}'$ and the total phase is just the line integral of the vector potential along C, i.e.,

$$\theta(\mathbf{r}', \mathbf{r}) = -\frac{e}{\hbar} \int_{C(\mathbf{r} \to \mathbf{r}')} \mathbf{A}(\mathbf{R}) \cdot \mathbf{u}(\mathbf{R}) dt. \tag{3}$$

$\mathbf{R}$ is a point on the curve C parameterized by the variable t (See Ref. 6 for details).

Secondly, this zero field Dirichlet Green's function is simplified to the 2D Green function for free propagation using the method of images.

$$G^+(x', y'; x, y) = e^{i\theta_1(\mathbf{r}', \mathbf{r})} G^F(x', y'; x, y) - e^{i\theta_2(\mathbf{r}', \mathbf{r})} G^F(x', y'; -x, y) \tag{4}$$

Here $\theta_1(\mathbf{r}',\mathbf{r})$ and $\theta_2(\mathbf{r}',\mathbf{r})$ are the phases accumulated for the Green function propagated to a point $\mathbf{r}'$ from a source at $\mathbf{r}(x,y)$ and its image at $\mathbf{r}''(-x,y)$ respectively (see Fig. 5 in Ref. 6).

The free Green function (wave function of a freely propagating particle emanating from a point source) in two-dimensions is the Hankel function of first kind of index zero whose asymptotic form looks like a cylindrical wave

$$G^F(r) = -\frac{m^*}{2\hbar} i H_0^{(1)}(kr) \approx \left[\frac{2}{\pi kr}\right]^{1/2} e^{i(kr-\frac{\pi}{4})}, \quad \text{if } kr \gg 1 \tag{5}$$

Putting this all together in Eq. 1 (supplementary), the wave function at the detector far away from the source (Fraunhofer regime) for small magnetic field is

$$\psi(r,\theta) = \left[-\left|\frac{k}{2\pi}\right|^{1/2} e^{-i\pi/4} e^{i(kr_0+\theta_0)}\right] \frac{\cos\theta}{\sqrt{r}} \int_{-\infty}^{\infty} dy \phi(0,y) e^{-i(ky\sin\theta - \frac{eBLy}{2\hbar})} \tag{6}$$

This more rigorous analysis leads us, apart from an unimportant constant in the bracket, to the same expression for $\psi(r,\theta)$ as we had in Eq. 2 (main text). The value of the wave function at the $x = 0$ boundary $\phi(0,y)$ [Eq. 1 (supplementary)] is the aperture function in Eqs. 1 and 2 (main text).

B. Complication due to $W \gg \lambda_F$ condition not being satisfied

The above analysis is mathematically consistent within the approximations used (far field, non-quantizing magnetic field) if the width of the slit is much larger than the Fermi wavelength of electrons. If this condition is not satisfied, the problem is not simple anymore. Sommerfeld and others have found approximate solutions for the corresponding electrodynamics problem[7,9] but it assumes that the wall separating the left and the right half planes is infinitesimally thin along the x-direction and the solution depends on matching the wave functions on the left- and the right-half planes at the $x = 0$ boundary.

In our actual experiments, width of the QPC along the x-direction is non-negligible and the passage of the electron from the left half-plane to the right half-plane involves a quasi-one dimensional propagation along the finite length of the QPC wave guide. Furthermore, the QPC width (W) is also not uniform and is expected to be larger at the exit than at the centre of the QPC. While propagating from the left-half plane to the right-half plane, the electron first goes through an adiabatic passage within the quasi-1D QPC and then a

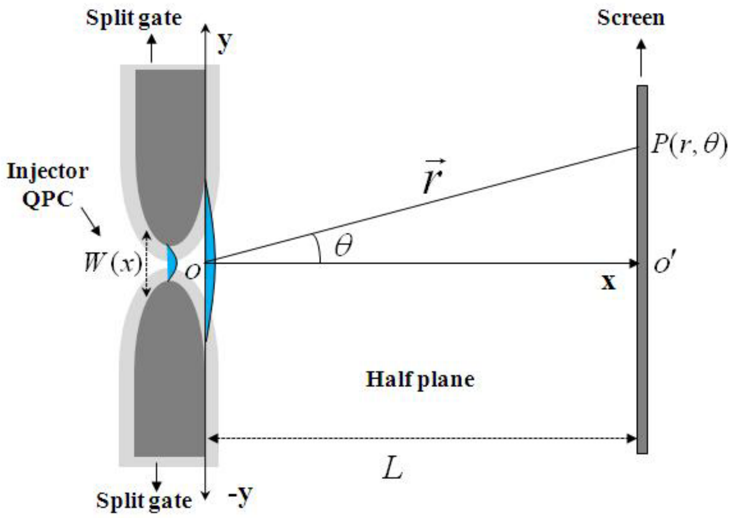

FIG. 5: (supplementary) Geometry for the Green function analysis. The value of the wave function at $x = 0$, $\phi(y, 0)$ completely determines its propagation in the right half-plane. Adiabatic propagation of the transverse eigenfunction through the exit of the QPC corresponding to single mode is indicated. The shaded region around the split gate represents the region of reduced electron density or reduced wave vector ($k'_F < k_F$), caused by the electrostatic gate voltage.

1D-to-2D dimensional crossover as it leaves the QPC. Unfortunately, none of these details are experimentally accessible and therefore it is meaningless to attempt a numerical solution of the problem.

So instead, we have again followed Saito, et al.[6] in assuming that the aperture function determining the wave function at the boundary is simply the sum of the various possible transverse wave guide modes, assuming that the QPC boundary is impenetrable. But unlike Saito, et al, we have considered intermode interference terms in the analysis as keeping these terms explained the features in the data better.

If we treat QPC as a waveguide, the aperture functions $\phi(0, y)$ can be approximated by transverse eigenfunctions of the various propagating modes. For a hard-walled passage the transverse eigenfunctions $\phi_\alpha(0, y)$ for odd and even modes, are trivially

$$\phi_\alpha(0,y) = \begin{cases} \sqrt{\frac{2}{W}}\cos(\frac{\alpha\pi y}{W}), & \text{if} -\frac{W}{2} \leq y \leq \frac{W}{2} \text{ and } \alpha = 1,3,5,.. \\ 0, & \text{otherwise} \end{cases} \tag{7}$$

$$\phi_\alpha(0,y) = \begin{cases} \sqrt{\frac{2}{W}}\sin(\frac{\alpha\pi y}{W}), & \text{if} -\frac{W}{2} \leq y \leq \frac{W}{2} \text{ and } \alpha = 2,4,6,.. \\ 0, & \text{otherwise} \end{cases} \tag{8}$$

It is reasonable to assume that the transverse eigenfunctions remain unaffected by the small magnetic field and there will not be any mode hopping at very low temperature. If the change in the width $W(x)$ of the QPC is a smooth and slowly varying function of x, one may further assume adiabatic propagation of the transverse wave functions from the centre of the QPC where $W(x)$ is minimum toward the exit of the QPC where it meets the right-half plane [Fig. 5 (supplementary)]. The condition of adiabatic passage at ultralow temperature implies that while the mode occupancy is determined by the minimum QPC width, the effective width appearing in the aperture function $\phi(0,y)$ may be considerably larger. The experimentally inferred W would obviously be the QPC width where it meets the 2DEG and not the width at the centre of the QPC.

As a consequence of the equipartition of current, the diffraction pattern at a distant point is the superposition of all the allowed modes for a given QPC width[10]. The diffraction intensity is simply

$$I = |\psi(r,\theta,B)|^2 \propto |\sum_\alpha f_\alpha(\theta,B)|^2 \tag{9}$$

where $f_\alpha(\theta,B) = \frac{1}{2i}[e^{i\frac{\pi\alpha}{2}}F(k_{y\alpha} - \delta') - e^{-i\frac{\pi\alpha}{2}}F(k_{y\alpha} + \delta')]$ and the function $F(k_{y\alpha} \pm \delta') = \sqrt{W}\text{sinc}[\frac{W}{2}(k_{y\alpha} \pm \delta')]$ with $k_{y\alpha} = \frac{\pi\alpha}{W}$ and $\delta' = k\sin\theta - \frac{eBL}{2\hbar}$.

III. CONDUCTANCE QUANTIZATION AND MODE STRUCTURE

The fact that $2e^2/h$ quantization steps in the QPC conductance are not observed [Fig. 2 (supplementary)] despite a very long mean free path and very low measurement temperature is not surprising. It is well-documented that there is an optimal channel length L_{opt}

$$L_{opt} \approx 0.4\sqrt{W\lambda_F} \tag{10}$$

for the observation of quantized conductance.[11] W the width and λ_F, the Fermi wavelength. With the experimentally inferred values of $W \sim 500$nm and $\lambda_F \sim 75$nm, $L_{opt} \approx 75$nm. The fact that the electron density is depleted within the channel would make λ_F and consequently L_{opt} even larger. In our experiment, the lithographically deposited metal top gate has a length of about 65nm. The actual situation is between an orifice and a well defined channel.

One must then ask whether (i) a value of $k_F W/\pi$ can still be meaningfully inferred from the measured conductance values, and (ii) if one may invoke the notion of modes in the analysis, as we have done.

Firstly we note that the formula for the conductance G

$$G = \frac{2e^2}{h}\left[\frac{2W}{\lambda_F}\right] \tag{11}$$

can also be derived *classically* for a narrow orifice in a thin wall separating two semi-infinite planes, as one would do for a Knudsen effusion cell [Eq. (2) on page 23 of Ref. 11]. To obtain Eq. (11) one does not need to explicitly invoke the quantum mechanics of electron propagation in a waveguide. The only difference between the quantum mechanical and the classical derivations is that quantum mechanically for propagating waveguide modes in a long channel, G is quantized in steps whereas classically G is a smooth function of W. The two formulae are identical when $N = 2W/\lambda_F$ is an integer. Hence the product $k_F W/\pi$ can be inferred from the measured values of G, even for a classical orifice. The only errors involved in this estimation are due to the contributions of evanescent modes and the reflections that may occur within the waveguide.

Secondly note that the actual observation of conductance quantization steps is a much more stringent requirement than the actual existence of modes at the QPC exit. In particular, the observation of quantized conductance is fundamentally dependent on the cancelation of the electron group velocity with the one-dimensional density of states.[11] If the one-dimensional channel is not well-defined, as in the case of short QPCs, one may not observe quantization steps. But this in itself does not forbid the formation of modes, which only depends on transverse boundary conditions imposed on the electron wave function by the QPC. As long as one can ignore evanescent modes (the QPCs are long enough to ignore them),[13] it is reasonable to assume that the wave functions of the electrons at the QPC exit are of the type described by Eqs. 7 and 8 (supplementary).

IV. ON THE EXPERIMENTALLY INFERRED VALUES OF W

The effective slit width W from the fits in Fig. 3 (a), 3(c), and 3(e) (main text) are found to be 511, 673 and 693 nm respectively. These W_{exp}'s are larger compared to what is expected from the measured conductance[4] and the electron density inferred from Hall effect and magnetic focussing experiments. This fact can be readily reconciled with if the real experimental conditions are taken into account. One of the reasons, the adiabatic passage of electrons from the centre of the QPC to its exit where its width is large, was already discussed above.[6,13] Secondly, region around the QPC orifice will have not same wave vector k_F all over. Due to the electrostatic top-gate[12] voltage V_g this region around the QPC will necessarily have a reduced and spatially-inhomogenous electron density, determined also by the split gate geometry.[11] For a reduced wave vector $k'_F(< k_F)$, one would infer a larger QPC width because, for a fixed number of modes N, $N \simeq \frac{k_F W}{\pi} = \frac{k'_F W_{exp}}{\pi}$. Thus W_{exp} should be taken to be more of a fit parameter whose actual value is dependent on the real experimental conditions. Critically, the choice of the number of modes $N = k_F W/\pi$, the other input used to fit the data in Fig. 3 (main text), is insensitive to these details as they were inferred from the measured value of the conductance.

1 B. J. van Wees, H. van Houten, C. W. J. Beenakker, J. G. Williamson, L. P. Kouwenhoven, D. van der Marel and C. T. Foxon, Phys. Rev. Lett. **60**, 848 (1988).

2 T. Ando, Phys. Rev. B **44**, 8017 (1991).

3 E. G. Haanappel and D. van der Marel, Phys. Rev. B **39**, 5484 (1989).

4 M. A. Topinka, B. J. LeRoy, S. E. J. Shaw, E. J. Heller, R. M. Westervelt, K. D. Maranowski and A. C. Gossard, Science **289**, 2323 (2000).

5 L. W. Molenkamp, A. A. M. Staring, C. W. J. Beenakker, R. Eppenga, C. E. Timmering, J. G. Williamson, C. J. P. M. Harmans and C. T. Foxon, Phys. Rev. B **41**, 1274 (1990).

6 M. Saito, M. Takatsu, M. Okada and N. Yokoyama, Phys. Rev. B **46**, 13220 (1992).

7 J. D. Jackson, Classical Electrodynamics, second edition(1975), sec. 9.8.

8 Y. Aharonov and D. Bohm, Phys. Rev. **115** , 485-491 (1959).

9 A. Sommerfeld, Optics(German edition 1950, English translation: Academic Press, 1964), Chap VI.

10 K. Kawamura, T. Ueta, H. Sawano, Jpn. J. Appl. Phys. **31**, 317-326 (1992).

11 H. van Houten, C. W. J. Beenakker, and B. J. van Wees, in Semiconductors and Semimetals, edited by M. A. Reed (Academic, New York, 1992), pp. 9-112.

12 S. Roddaro, V. Pellegrini, F. Beltram, G. Biasiol, L. Sorba, Phys. Rev. Lett. **93**, 046801-4

(2004).

[13] L. I. Glazman, G. B. Lesovik, D. E. Khmel'nitskii, and R. I. Shekhter, JETP Lett 48, 238 (1988).